

Recent progress in graphene terahertz modulators

Xieyu Chen(陈勰宇), Zhen Tian(田震), Quan Li(李泉), Shaoxian Li(李绍限), Xueqian Zhang(张学迁), Chunmei Ouyang(欧阳春梅), Jianqiang Gu(谷建强), Jiaguang Han(韩家广), Weili Zhang(张伟力)

Citation: Chin. Phys. B . 2020, 29(7): 077803 . **doi:** 10.1088/1674-1056/ab9433
Journal homepage: http://cpb.iphy.ac.cn; http://iopscience.iop.org/cpb

What follows is a list of articles you may be interested in

Single-shot measurement of THz pulses

Lei Yang(杨磊), Lei Hou(侯磊), Chengang Dong(董陈岗), Wei Shi(施卫)

Chin. Phys. B . 2020, 29(5): 057803 . **doi:** 10.1088/1674-1056/ab821f

Non-perturbative multiphoton excitation studies in an excitonic coupled quantum well system using high-intensity THz laser fields

Monica Gambhir, Vinod Prasad

Chin. Phys. B . 2019, 28(8): 087803 . **doi:** 10.1088/1674-1056/28/8/087803

Optically induced abnormal terahertz absorption in black silicon

Dong-Wei Zhai(翟东为), Hai-Ling Liu(刘海玲), Xxx Sedao, Yu-Ping Yang(杨玉平)

Chin. Phys. B . 2018, 27(2): 027802 . **doi:** 10.1088/1674-1056/27/2/027802

Design and theoretical study of a polarization-insensitive multiband terahertz metamaterial bandpass filter

Hai-Peng Li(李海鹏), Wen-Yue Fu(付文悦), Xiao-Peng Shen(沈晓鹏), Kui Han(韩奎), Wei-Hua Wang(王伟华)

Chin. Phys. B . 2017, 26(12): 127801 . **doi:** 10.1088/1674-1056/26/12/127801

Optical response of tunable terahertz plasmon in a grating-gated graphene transistor

Bo Yan(闫博), Jingyue Fang(方靖岳), Shiqiao Qin(秦石乔), Yongtao Liu(刘永涛), Li Chen(陈力), Shuang Chen(陈爽), Renbing Li(李仁兵), Zhen Han(韩震)

Chin. Phys. B . 2017, 26(9): 097802 . **doi:** 10.1088/1674-1056/26/9/097802

TOPICAL REVIEW — Terahertz physics

Recent progress in graphene terahertz modulators*

Xieyu Chen(陈勰宇)[1], Zhen Tian(田震)[1,†], Quan Li(李泉)[1], Shaoxian Li(李绍限)[1], Xueqian Zhang(张学迁)[1], Chunmei Ouyang(欧阳春梅)[1], Jianqiang Gu(谷建强)[1], Jiaguang Han(韩家广)[1], and Weili Zhang(张伟力)[2,‡]

[1] *Center for Terahertz Waves and School of Precision Instrument and Optoelectronics Engineering, and the Key Laboratory of Optoelectronics Information and Technology (Ministry of Education), Tianjin University, Tianjin* 300072, *China*
[2] *School of Electrical and Computer Engineering, Oklahoma State University, Stillwater, Oklahoma* 74078, *USA*

(Received 27 March 2020; revised manuscript received 3 May 2020; accepted manuscript online 19 May 2020)

Graphene has been recognized as a promising candidate in developing tunable terahertz (THz) functional devices due to its excellent optical and electronic properties, such as high carrier mobility and tunable conductivity. Here, we review graphene-based THz modulators we have recently developed. First, the optical properties of graphene are discussed. Then, graphene THz modulators realized by different methods, such as gate voltage, optical pump, and nonlinear response of graphene are presented. Finally, challenges and prospective of graphene THz modulators are also discussed.

Keywords: terahertz, graphene, modulators

PACS: 78.67.Wj, 87.50.U–, 42.79.Hp **DOI:** 10.1088/1674-1056/ab9433

1. Introduction

Terahertz (THz) wave, situated between infrared and microwave regimes, is an important branch of electromagnetic spectrum. Compared to other wave bands, THz wave has many fascinating properties, suggesting promising applications in imaging, communication, and spectroscopy fields.[1] In the last two decades, breakthroughs in THz sources and detectors have greatly promoted the development of THz science and technology. However, owing to the shortage of advanced THz components, most applications can only be investigated and realized in laboratories. Among these, high performance THz modulators for manipulating the amplitude, phase, polarization, and propagation of the THz wave, are highly desirable in many fields, such as THz imaging and communications.[2,3] To meet the application requirements, THz modulators have been presented based on materials with tunable optical properties, such as bulk semiconductors,[4,5] two-dimensional materials,[6,7] liquid crystals,[8] superconductors,[9] and phase change materials.[10,11] Moreover, MEMS-based THz modulator has also been experimentally demonstrated.[12]

Graphene, as a two-dimensional semiconductor material, has attracted much attention due to its extraordinary electronic and optical properties[13] and has been widely applied in photonics, plasmonics and optoelectronics fields.[14,15] In recent years, graphene has also been used to modulate the properties of the THz wave.[16–35] Compared to other materials, graphene has many unique advantages: (i) ultrahigh carrier mobility on the order of 10^6 cm^2/(V·s).[36] (ii) The carrier concentration of graphene and thus its optical properties in the THz regime can be extensively modified by external stimulants, such as gate voltage[37] and optical pump.[38] (iii) The high quality large-area graphene can be realized by traditional chemical vapor deposition (CVD) method, which makes graphene easy to prepare and cost-effective. (iv) Graphene exhibits many other outstanding properties, such as broadband response, mechanical flexibility and compactness. However, because the wavelength of THz (1 THz = 300 μm) is much larger than the thickness of graphene, the interaction between the THz wave and graphene is limited. To solve the problem, resonant structures have been integrated into the graphene-based THz modulators[39–44] to further improve the modulation performance. Moreover, graphene plasmon based THz modulators have also been designed and demonstrated.[45,46]

In this review, we outline our recent work on graphene-based THz modulators. First, we briefly introduce the optical properties of graphene especially in the THz regime. Second, we show a passively controlled THz modulator based on graphene, which acts as a precursor for tunable devices. Then, several graphene-based THz devices modulated by gate voltage and simultaneous electric and optical stimulants are discussed. Additionally, we present a graphene-metal hybrid THz modulator based on the nonlinear interaction between strong THz field and graphene. Finally, the challenges and prospects of graphene-based devices for THz manipulation are also discussed.

*Project supported by the National Key Research and Development Program of China (Grant No. 2017YFA0701004) and the National Natural Science Foundation of China (Grant Nos. 61675145, 61722509, 61735012, and 61420106006).

†Corresponding author. E-mail: weili.zhang@okstate.edu

© 2020 Chinese Physical Society and IOP Publishing Ltd

2. Optical properties of graphene

Graphene is a single atom thick planar sheet with sp2 hybrid carbon atoms arranged in a hexagonal lattice. In recent years, graphene has been widely integrated into photonics, plasmonics and optoelectronic devices taking advantages of its extraordinary electronic and optical properties. These properties are inherited from the special energy band structure of graphene, which can be well calculated using a tight-binding model.[47] As shown in Fig. 1(a), the valence band and the conduction band are symmetric and contact each other at Dirac point, which means graphene is a gapless material. Moreover, near the Dirac point, electrons and holes in the graphene hold a linear dispersion relation. Its special energy band structure results in many peculiar properties, such as ultrahigh carrier mobility, a large scale tunable conductivity, and special optical properties, which make graphene a promising candidate for optical modulator applications.

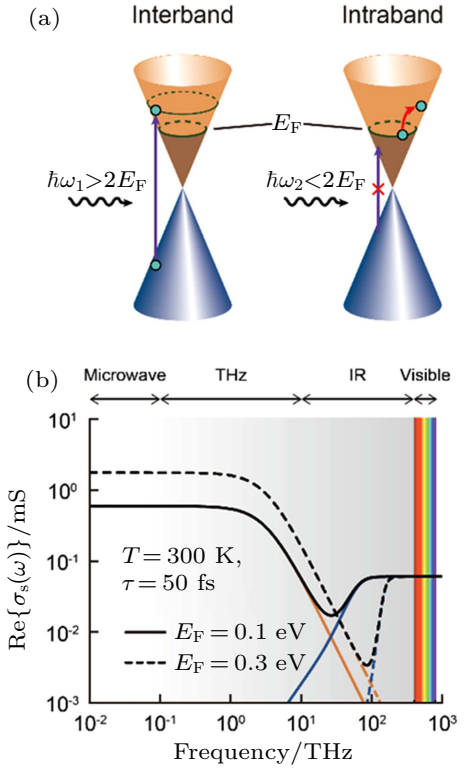


Fig. 1. (a) Energy band structure of graphene near the Dirac point and schematic diagrams of the possible optical transitions: interband (left) and intraband (right). (b) Real part of the surface conductivity from 10^{-2} THz to 10^3 THz in graphene with different Fermi levels. The contribution from intraband transitions and interband transitions are also plotted in orange and blue lines, respectively.

In general, absorption of electromagnetic waves can be described by the imaginary part of the permittivity of a material, which is associated with the real part of its surface conductivity. Moreover, the absorption results from the optical transition in the material, and thus the conductivity. As demonstrated previously,[48,49] intraband transitions and interband transitions in graphene can both contribute to the conductivity. Therefore, the surface conductivity of graphene can be expressed as the sum of the intraband conductivity and the interband conductivity

$$\sigma_s(\omega) = \sigma_{\mathrm{intra}}(\omega) + \sigma_{\mathrm{inter}}(\omega), \tag{1}$$

where

$$\sigma_{\mathrm{intra}}(\omega) = \mathrm{i}\frac{e^2}{\pi\hbar^2(\omega + \mathrm{i}\tau^{-1})} \times \int_0^{\infty} [f(\varepsilon - E_F) + f(\varepsilon + E_F)]\mathrm{d}\varepsilon, \tag{2}$$

$$\sigma_{\mathrm{inter}}(\omega) = \mathrm{i}\frac{e^2\omega}{\pi}\int_0^{\infty}\frac{f(\varepsilon - E_F) - f(-\varepsilon - E_F)}{(2\varepsilon)^2 - (\hbar\omega + \mathrm{i}\tau^{-1})^2}\mathrm{d}\varepsilon. \tag{3}$$

Here, $f(\varepsilon - E_F) = 1/(\exp[(\varepsilon - E_F)/k_B T] + 1)$ is the Fermi–Dirac distribution function with Fermi energy of E_F. Where k_B, T, e, and $\hbar$ are the Boltzmann constant, temperature, electron charge, and reduced Planck's constant, respectively. τ is the carrier relaxation time of graphene due to scattering. At high frequencies, such as near infrared and visible range, the photon energy is higher than $2E_F$. Therefore, the interband transitions occur and dominate the surface conductivity of graphene, as illustrated in the left panel of Fig. 1(a). At low frequencies, the surface conductivity is dominated by intraband transitions. On this condition, interband transitions are forbidden in graphene since the photon energy is much lower than $2E_F$, as shown in the right panel of Fig. 1(a).

To further understand the surface conductivity of graphene under different frequency ranges, the real part of surface conductivity with different Fermi levels is calculated and shown in Fig. 1(b). In the calculation, the temperature T is 300 K and the relaxation time τ is fixed at 50 fs, which can be easily reached in experiment.[29] The conductivity contribution of intraband transitions and interband transitions are also plotted. At very high frequencies, such as visible range, the surface conductivity of graphene reduces to a constant value of $e^2/4\hbar$, which is independent of the Fermi level of graphene. The constant conductivity results in a relatively low universal absorbance of $\sim 2.3\%$,[50] which makes graphene a potential material for transparent-flexible electrodes applications. In the infrared range, the conductivity of graphene is dominated by both intraband and interband transitions, and can be modified by modulating the Fermi level. Although the conductivity modification in this frequency range is relatively weak, several modulators and other tunable devices have been demonstrated experimentally.[51,52] In the THz and microwave regimes, the energy of photon is much lower than the Fermi level. Therefore, the surface conductivity of graphene is only dominated by intraband transitions and can be approximately expressed as a function of E_F by the Drude model[29]

$$\sigma_s(\omega) = \frac{e^2 E_F}{\pi\hbar^2}\frac{1}{\omega + \mathrm{i}\tau^{-1}}. \tag{4}$$

In this frequency range, as shown in Fig. 1(b), the conductivity of graphene can be extensively modulated by controlling the Fermi level. Thus, graphene is a suitable material for tunable THz devices, especially modulators.

3. Graphene-based THz modulators

In recent years, by electrically or optically controlling the Fermi level of graphene, some THz modulator devices have been experimentally demonstrated. Next, we will present a brief review of our recent progress in THz modulators by modifying the Fermi level and thus the conductivity of graphene in several different methods.

3.1. Passively controlled THz modulator

As discussed above, at THz frequencies, the conductivity of graphene can be extensively modified, which is highly desirable for modulator devices. However, the thickness of graphene (~ 0.35 nm) is much smaller than the wavelength of the THz wave. Therefore, the interaction between THz electric field and graphene is limited, and thus the performance of the modulator devices. To enhance the interaction between the THz wave and graphene, in recent years, metal-based resonators have been widely integrated into the graphene based modulator devices due to their ability of extreme field confinement.[16] Thus, it is important to fully understand the interaction between graphene and different resonant modes of metallic resonators since the passive response is the fundamental of modulator device design.

To investigate the influence of graphene on different resonant modes, we designed a metallic metasurface consisting of an array of THz asymmetric spit-ring resonators (TASRs),[53] as illustrated in Fig. 2(a). The metallic structures were deposited on a p-type silicon substrate by conventional photolithography. Next, the monolayer graphene grown by commercial CVD was transferred to the sample by wet-based transfer method. The TASRs structure can support two different resonant modes, Fano mode and dipole-like mode, both can be modified by changing the distance d between two capacitive gaps. Then, samples with different values of d before and after the graphene deposition were experimentally measured in a broadband (0.1 THz–4.5 THz) THz time-domain spectroscopy (THz-TDS) system.

Measured transmission spectra of different samples are shown in Figs. 2(b)–2(e). When the distance between the two gaps is $d = 0$ μm, the structure is symmetric and only dipole mode can be excited around 0.7 THz. This mode can also be seen as a symmetric mode with in-phase surface current in two split ring resonators of TASR.[54] Therefore, the radiative coupling between the mode and free space is strong, which results in a broad resonance line width and relatively low field confinement in gaps. By increasing d from 0 μm to 20 μm, the intrinsic symmetry of the structure is broken, and an asymmetric resonant mode, named as Fano mode, can be supported at 0.5 THz. The surface current in two split ring resonators are out of phase and thus can cancel each other. Therefore, this sharp resonance is weakly coupled to the free space and the THz field enhancement in gaps is much higher compared to the dipole mode.

When a monolayer graphene is transferred onto the sample, the dipole mode does not exhibit a significant change in the resonance profile of all the samples. While the Fano mode undergoes a large decrease in the resonance strength, which can be attributed to the strong interaction between the highly confined THz electric field in gaps and the monolayer graphene. Moreover, the modulation performance of graphene becomes more significant with d increased from 0 μm to 20 μm. Numerical simulations were also performed using commercial full-wave numerical software CST Microwave Studio, as illustrated in Figs. 2(f)–2(i), which agree well with the experiment. According to the discussion, we conclude that the interaction between THz and graphene can be significantly enhanced by resonant modes with high electric field confinement, which can be applied in design of advanced graphene-based THz modulators.

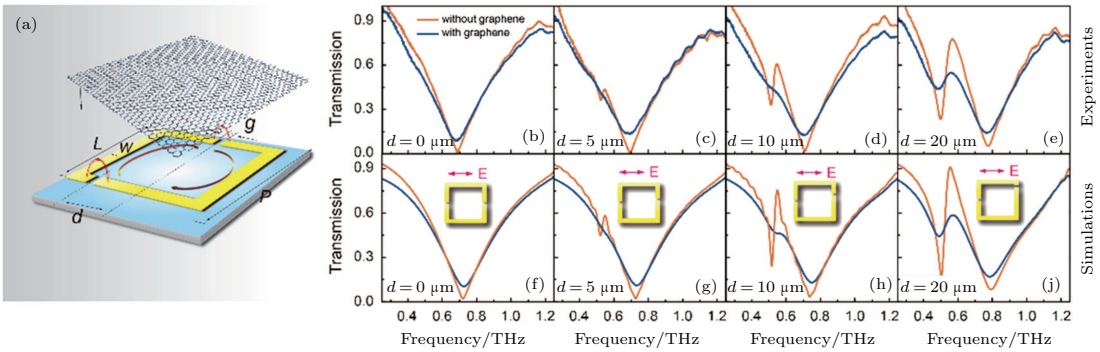


Fig. 2. (a) Schematic view of the unit cell of the Fano resonant metasurface, which consists of an array of THz asymmetric spit-ring resonators. Measured [(b)–(e)] and simulated [(f)–(i)] transmission spectra of metasurface with different values of d before (orange lines) and after (blue lines) the graphene deposition. The polarization of the incident THz electric field is vertical to the gaps. Figure reprinted with permission: Ref. [53], ©2016 by the Royal Society of Chemistry.

3.2. Electrically controlled THz modulator

As a two-dimensional gapless material, the carrier concentration and optical properties of graphene can be changed widely by external stimulants, such as optical pump, gate voltage, and chemical doping.[55] Among the methods, electrical modulation has advantages including flexibility and reversibility, which has been widely adopted in graphene-based modulator devices. At first, to modulate the Fermi level of graphene, a conventional field effect transistor (FET) was designed.[17] However, the capacitance of such devices is relatively small due to the high thickness of the insulating layer and the limited dielectric constant. Thus, the bias voltage used to modulate the carrier concentration of graphene was always too high, sometimes even reached several hundred volts,[16] which extensively constrains the practical application of graphene-based THz modulators. Recently, by replacing the insulation layer of FET structure with ionic liquid[25] or ion gel,[39] the Fermi level of graphene can be effectively modulated by a small gate voltage, which can be attributed to the electrical double layer (EDL) formed next to the interface between graphene and electrolyte. Several graphene-based modulators have been experimentally demonstrated based on this method and showed attractive modulation performance.[27,28,41]

While most of graphene THz modulators were transmission-based, the reflection-type modulators, such as Salisbury screen structure,[56,57] can show richer properties resulted from the interference between the incident and reflected THz waves. However, the carrier concentration needed to realize near zero reflection is relatively high in such devices due to low quality of CVD-grown graphene. To resolve this problem, we integrated metallic gratings into the classical Salisbury screen structure based on graphene,[58] as shown in Fig. 3(a). The Fermi level of graphene was electrically modulated by ion gel electrolyte. The details of sample fabrication process were described in Ref. [58]. Then the samples were experimentally characterized using a broadband fiber-based THz time-domain spectroscopy system.

Measured reflection spectra with different gate voltages of samples without (sample A) and with (sample B) metallic grating are shown in Figs. 3(b) and 3(e), respectively. It can be observed that the resonance frequencies of samples A and B are 0.75 THz and 0.43 THz, respectively. The shift of resonance frequency can be attributed to the effective optical parameter change of graphene layer induced by the metallic grating structure. At the resonance, the reflection of both samples can be modulated to zero, indicating a 100% modulation depth. The reflection coefficient *versus* gate voltages at resonance frequencies of two samples were further extracted and illustrated in Figs. 3(c) and 3(f). Though 100% modulation can be realized in both samples, the gate voltage needed for zero reflection in sample B is closer to the charge neutral point. It indicates that the perfect absorption can be reached under a relatively small conductivity of graphene. This can be qualitatively explained by the THz electric field enhancement ability of metallic grating structure. The absorbance at the resonance and modulation depth were also calculated for both samples, as shown in Figs. 3(d) and 3(g). Ion gel electrolyte based electric modulation is an efficient method for graphene THz modulator applications. Moreover, the integration of plasmonic structures can significantly improve the performance of modulators and increase the degree of design.

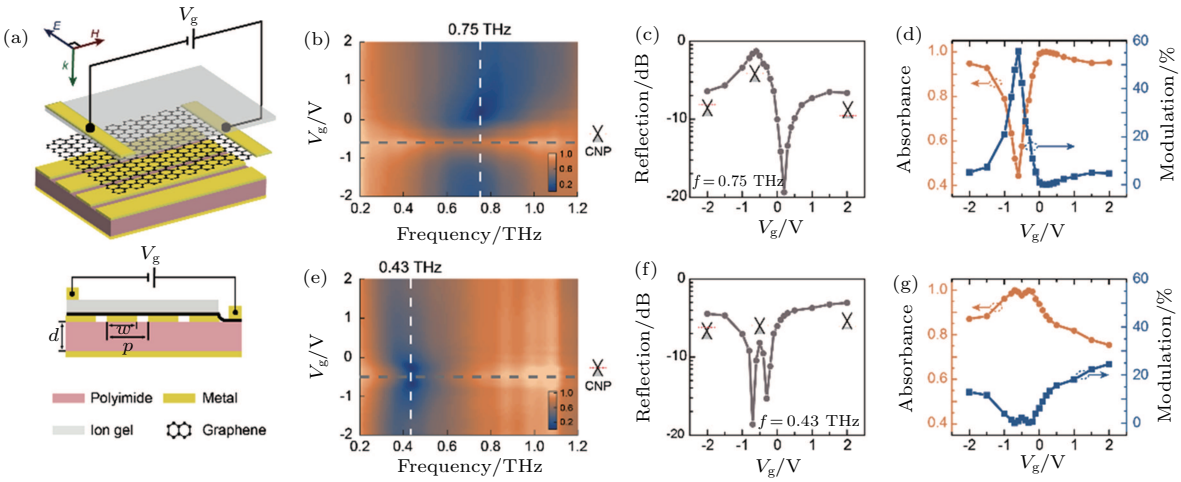


Fig. 3. (a) Schematic diagram of the graphene and metallic grating-based reflective THz modulator gated by the ion gel (top panel) and the side view of the device (low panel). Measured reflection spectra under different gate voltages (b) without the metallic grating and (e) with the metallic grating. The resonance frequency and charge neutral points (CNP) are plotted by the white and gray dash lines. Extracted reflection coefficient under different gate voltages at resonance frequency (c) without the metallic grating and (f) with the metallic grating. Calculated absorbance and modulation depth at resonance frequency (d) without the metallic grating and (g) with the metallic grating.[58] Figure reprinted with permission: Ref. [58], ©2019 by the John Wiley and Sons.

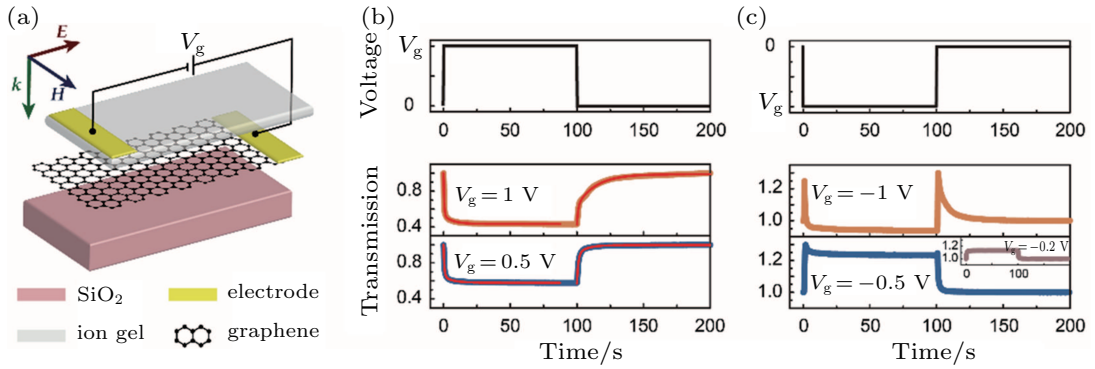


Fig. 4. (a) Schematic diagram of the ion gel gated graphene THz modulator. (b) Positive square-wave voltage applied to the graphene (top panel) and time response of the modulator under 1-, 0-, and 0.5-V gate voltages (low panel). Red lines show the results of fitting. (c) Negative square-wave voltage applied to the graphene (top panel) and the time response of the modulator under −1.0-V, −0.5-V, and −0.2-V gate voltages (low panel), respectively.[59] Figure reprinted with permission: Ref. [59], ©2019 by the Elsevier Publisher.

Table 1. Retrieved time constants of two processes.

Time constant	0 V–1 V		0 V–0.5 V	
	Fall/s	Rise/s	Fall/s	Rise/s
τ_1	0.48	0.94	0.63	1.04
τ_2	7.06	14.00	7.34	7.24

Though a great number of ion gel-gated graphene modulators in the THz regime were reported, the modulation speed of such devices remained unexplored, which is an important performance criterion of modulator for practical applications. To investigate the modulation speed of gated graphene modulator, we designed and fabricated a simple prototype.[59] As shown in Fig. 4(a), a CVD-grown monolayer graphene was transferred onto a quartz substrate followed by electrodes fabricated and ion gel coated. The temporal response of the sample was characterized in a continuous wave THz system with 100 GHz, as described in Ref. [59]. Measured THz power transmission as a function of time and corresponding gate voltage wave forms are shown in Figs. 4(b) and 4(c). When the positive voltage is applied, as the gate voltage switches back to 0 V, the transmission power decreases and then returns the initial value. However, when the gate voltage is switched to a negative value larger than CNP, the transmission power increases first and then decreases indicating that the Fermi level has passed through the Dirac point, as illustrated in the low panel of Fig. 4(c). To fit the dynamic change of the modulator, a double-exponential function with two relaxation processes was used

$$T(t) = A_0 + A_1 \mathrm{e}^{-(t-t_0)/\tau_1} + A_2 \mathrm{e}^{-(t-t_0)/\tau_2}, \tag{5}$$

where τ_1 and τ_2 are the time constant of two processes, respectively. The fitting results are shown in the low panel of Fig. 4(b) as red lines and the retrieved time constants are summarized in Table 1. According to the results, we can conclude that the modulation speed of modulator is on the scale of second and constrained by two kinds of mechanisms. One is the fast decay process which can be attributed to the slow ion mobility in the ion gel.[60] The slow process may origin from the charge trapping at grain boundaries and defect points due to non-idealities in graphene grown or sample fabrication.[16] Although ion gel can be used to efficiently modulate the Fermi level of graphene, the modulation speed is relatively slow. In the future, we can further improve the modulation performance by choosing ion gel with faster polarization response or optimized the geometry properties of such devices.

3.3. Electrically and optically controlled THz modulators

Besides electrical modulation, optical pump is also a common method to modify the Fermi level of graphene. By transferring graphene directly onto the semiconductor substrate, optically controlled THz modulators have been experimentally demonstrated.[31,32] When an optical excitation is illuminated on the surface of graphene-semiconductor structure, large density of free carriers is generated within a volume defined by the penetration length of the optical beam in substrate and diffused into graphene layer, which leads to the conductivity change of graphene and also the transmission of THz signal. On this basis, we introduced gate voltage into the structure which can further drive the photo-induced carriers and improve the performance of graphene-based THz modulator.[61] Our design is schematically illustrated in Fig. 5(a). Periodically arranged split-ring resonators were integrated between the graphene and semiconductor substrate to enhance the interaction between graphene and THz wave. Two square-ring electrodes were designed and fabricated onto the top and bottom surface of the modulator to apply gate voltage without blocking THz wave. The sample was measured using a broadband THz-TDS system with a uniform optical excitation of continuous wave laser beam at 532 nm.

Measured transmission spectra of the metasurface modulator under different gate voltages are shown in Fig. 5(b). A transmission dip can be observed approximately at 0.67 THz which origins from the LC resonance mode of the split-ring resonator. Under the photoexcitation, as the gate voltage increases from 0 V to 5 V, the transmission is enhanced first and reaches the maximum at $V_g = 1$ V where the Fermi level of graphene is next to the Dirac point. With further increase in V_g, a decreasing trend of transmission can be observed. On the other hand, as the gate voltage is changed from 0 V to −5 V, the transmission undergoes a significant decrease. Such modulation behavior is dominated by the optical properties of graphene layer and can be well explained by the shift of Fermi level of graphene under different gate voltages. When a positive voltage is applied, the photo-induced electrons are drifted from silicon structure into the graphene layer. However, since the graphene is p-doped in air, the Fermi level rises toward the Dirac point at first, which leads to the increase in THz transmission. After the Fermi level has passed through the Dirac point, the transmission starts to decrease with Vg increased. While, as a negative voltage is applied, the photo-induced holes are drifted into the graphene sheet. Therefore, the Fermi level monotonically moves down from initial position, thus the transmission of THz decreases. By extracting the transmission coefficient at resonant frequency, the modulation behavior of such device can be observed more clearly, as shown in Fig. 5(c).

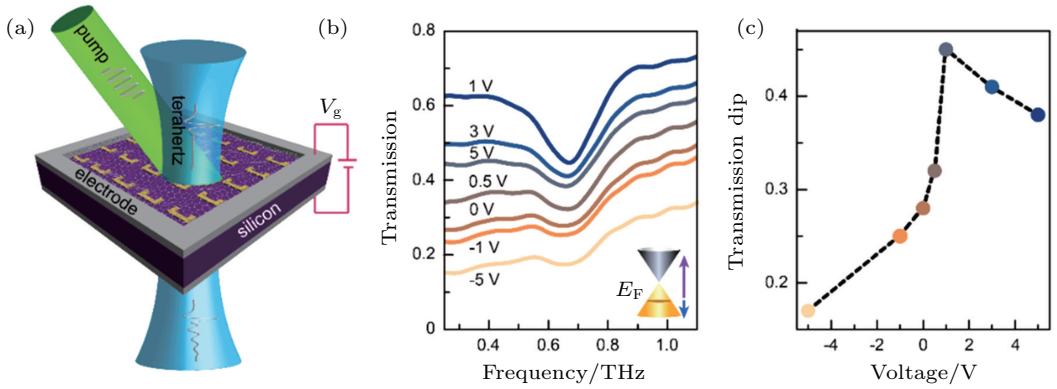


Fig. 5. (a) Schematic view of graphene and split-ring resonator hybrid metasurface modulator. (b) Measured transmission spectra under 532-nm, 280-mW light illumination with different gate voltages. The energy band structure and Fermi level of graphene are shown in the inset. (c) Extracted transmission coefficient as a function of gate voltage at resonant frequency.[61] Figure reprinted with permission: Ref. [61], ©2015 by the Elsevier Publisher.

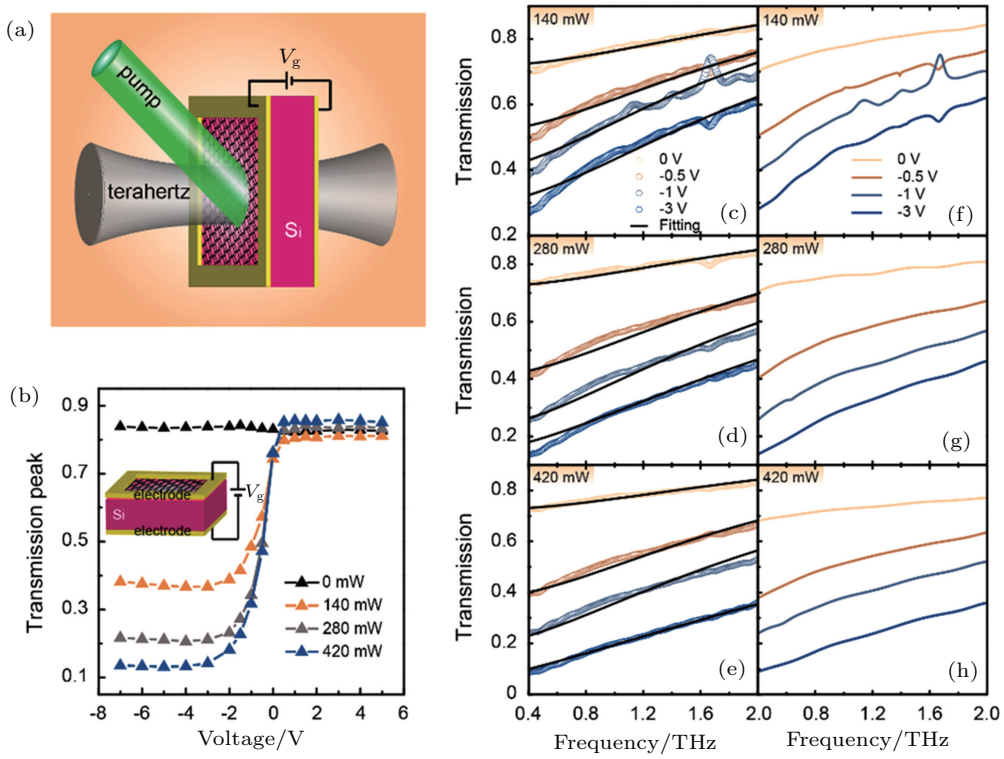


Fig. 6. (a) Schematic diagram of double-layer graphene-based THz modulator. (b) Measured transmission of the peak THz field as a function of gate voltage under different photoexcitation powers (continuous wave laser at 532 nm). Measured (c)–(e) and simulated (f)–(h) transmission with different gate voltages under photoexcitation power of 140, 280, and 420 mW, respectively.[62] Figure reprinted with permission: Ref. [62], ©2015 by Springer Nature.

However, due to the resonant properties of the split-ring structure, the modulation depth of such device is related to the frequency, which severely constrains its broadband applications. To address the problem, we presented a graphene based broadband THz modulator without integrating any resonant structures,[62] as illustrated in Fig. 6(a). With simultaneous electrical and optical excitations, an 83% transmission modulation and broadband response from 0.2 THz to 2 THz were experimentally demonstrated. It should be mentioned that, in order to improve the modulator performance, two layers of graphene were transferred onto an n-type silicon substrate in turn, instead of one layer. The sample was illuminated by a 532-nm continuous wave laser beam and electrically gated using two square-ring electrodes on the bottom and top of the sample. A broadband THz-TDS system was adopted to characterize the modulator performance.

Measured transmission coefficient of peak THz field versus gate voltage under different photoexcitation powers is shown in Fig. 6(b). Under photoexcitation of the green laser, many photo-induced carriers are generated in a thin layer of silicon substrate beneath the graphene. Compared with the n-type silicon substrate, the graphene layer acts as a 'p-type' material. Thus, the photo-induced electrons will diffuse from silicon substrate to the graphene layer until the equilibrium state is reached, leading to the formation of a depletion layer next to the graphene. This configuration is an analogue of a 'PN' junction structure. When a positive voltage is applied, a current flow can be formed in the electric circuit. Under the circumstances, it is hard for electrons to accumulate in graphene, thus the transmission of THz almost remains unchanged. While, as the gate voltage is swept from 0 V to −7 V, the depletion layer is broadened and electrons will be injected into the graphene layer. As a result, the transmission gradually decreases and reaches a saturation point at around −4 V for all the photoexcitation power. Moreover, the transmission of THz can be modulated in a broadband ranging from 0.4 THz to 2 THz, as illustrated in Figs. 6(c)–6(e). It should also be noted that, as demonstrated in the previous works,[63,64] the modulation properties of such device are associated with the semiconductor material of substrate which should be further investigated to improve the modulator performance. As discussed above, an efficient graphene-based THz modulator can be realized under simultaneous optical excitation and a low voltage bias, which is highly desirable in future THz applications.

3.4. Intensity based THz modulator

So far, we have only discussed the modulator devices based on the linear interaction between graphene and low THz electric field wherein the modulation is realized by electrically or optically changing the carrier concentration of graphene. Furthermore, as demonstrated previously,[65,66] the conductivity of graphene can also be tuned by changing electric field intensity in the frame of nonlinear interaction with high THz field, due to the modification of the scattering time τ in graphene. By taking advantage of the nonlinear response of graphene in the THz regime, we presented an electric field modulated device,[67] as schematically illustrated in Fig. 7(a). The modulator is composed of a CVD-grown single-layer graphene, an array of three orthogonally oriented SRRs and a sapphire substrate. The metal structures can significantly enhance the electric field in gaps, and thus the interaction between graphene and THz wave. To test the modulation performance of such device, the linear response of the samples with or without graphene coated was measured in a commercial THz-TDS system. The nonlinear transmission spectra of the sample coated with graphene was characterized in a $LiNbO_3$ based home-build strong-field THz system.

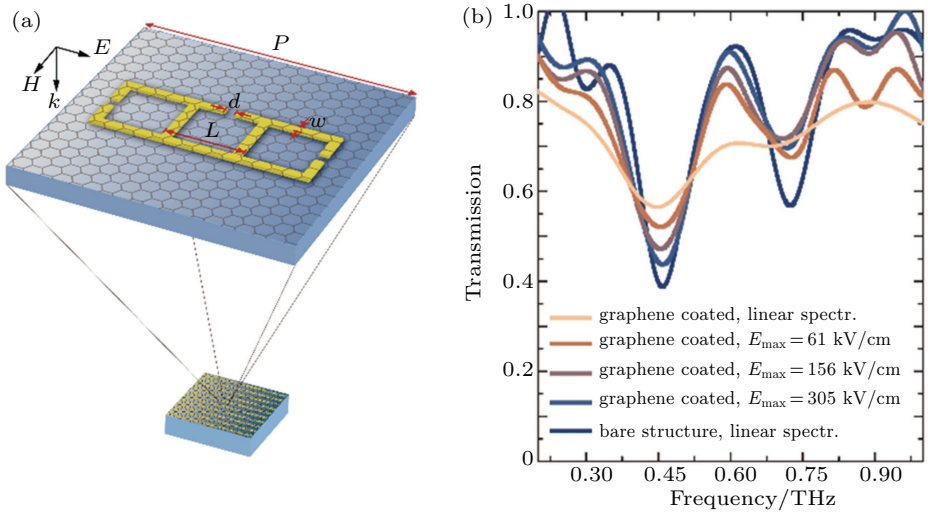


Fig. 7. (a) Schematic view of the graphene–metal hybrid metasurface. (b) Measured transmission spectra of the sample with and without graphene layer under different THz electric field intensities.[67] Figure reprinted with permission: Ref. [67], ©2019 by the Optical Society of America (OSA).

As shown in Fig. 7(b), two resonances at 0.45 THz and 0.7 THz, corresponding to anti-symmetric and symmetric modes, can be observed in the uncoated sample, which arise from the near-field coupling between three SRRs. When a single-layer graphene is transferred onto the metal structure, the damping of the resonant modes in three SRRs increases leading to the weakening of the two hybrid resonances. Then the coated sample was measured under three different THz field intensities of 61 V/cm, 156 V/cm, and 305 V/cm. Unlike in the linear regime, the resonance strength of both modes is enhanced with increasing field intensity. It indicates that the conductivity of graphene is lower under high THz field intensity, which is consistent with the argument in previous works.[66] As the THz intensity is switched to 305 V/cm, a maximum modulation depth of 23% is achieved which can be further improved by introducing extra electrical modulation into the device.

4. Conclusion and perspectives

We summarized our recent progress in graphene-based THz modulators. The modulation was realized by changing the conductivity of graphene using different approaches, including gate voltage, optical pump, and nonlinear response of graphene under strong THz field. To further improve the modulation performance of such devices, resonant structures were carefully designed and integrated into the modulators due to their ability of enhancing the interaction between graphene and THz wave. The works reviewed here present only a small step to design advanced THz modulators.

Compared to other materials used in THz modulators, such as bulk semiconductors, liquid crystal, other two-dimensional materials, and phase change materials, graphene has many benefits, such as ultrahigh carrier mobility, extensively tunable conductivity, broadband response and stability, which makes graphene a potential candidate for THz modulators applications. However, there are still some blocks in further improving the modulation performance of such devices. (i) The quality of CVD-grown graphene is limited with relatively low carrier mobility, which extensively constrains the modulation ability of graphene for both modulation and plasmonics applications. (ii) The modulation speed is still not high enough for many THz technology, such as THz spatial light modulators (SLM)[68] and THz compressive imaging.[69] In fact, the modification of graphene conductivity in such modulators was mainly realized by traditional capacitor configuration, which indicates that the modulation speed of these devices was constrained by RC time constant limitations. Therefore, in the future, the switching speed can be further improved by decreasing the active area of graphene or optimizing the architectures of modulators, both of which will significantly reduce the RC time constant of the graphene-based devices. (iii) Certain interaction mechanisms between graphene and other structures remain unexplored which can also be further investigated to improve the performance of graphene-based modulators. If the remaining problems can be addressed, graphene-based THz modulators may be utilized in many THz technologies, such as THz imaging, spectroscopy and communication. In the future, further improvement of such devices will be the key for advancing THz technology.

References

[1] Tonouchi M 2007 *Nat. Photon.* **1** 97
[2] Kleine-Ostmann T and Nagatsuma T 2011 *J. Infrared Millimeter Terahertz Waves* **32** 143
[3] Mittleman D M 2018 *Opt. Express* **26** 9417
[4] Lim W X, Manjappa M, Srivastava Y K, Cong L, Kumar A, MacDonald K F and Singh R 2018 *Adv. Mater.* **30** 1705331
[5] Wen T, Zhang C, Zhang X, Liao Y, Xiang Q, Wen Q, Zhang D, Li Y, Zhang H, Jing Y and Zhong Z 2018 *Opt. Lett.* **43** 3021
[6] Chanana A, Liu X, Zhang C, Vardeny Z V and Nahata A 2018 *Sci. Adv.* **4** eaar7353
[7] Hu Y, Jiang T, Zhou J H, Hao H, Sun H, Ouyang H, Tong M Y, Tang Y X, Li H, You J, Zheng X, Xu Z J and Cheng X G 2020 *Nano Energy* **68** 104280
[8] Savo S, Shrekenhamer D and Padilla W J 2014 *Adv. Opt. Mater.* **2** 275
[9] rivastava Y K, Manjappa M, Cong L, Krishnamoorthy H N S, Savinov V, Pitchappa P and Singh R 2018 *Adv. Mater.* **30** 1801257
[10] Zhao Y C, Zhang Y X, Shi Q W, Liang S X, Huang W X, Kou W and Yang Z Q 2018 *ACS Photon.* **5** 3040
[11] Cai H L, Chen S, Zou C W, Huang Q P, Liu Y, Hu X, Fu Z P, Zhao Y, He H C and Lu Y L 2018 *Adv. Opt. Mater.* **6** 1800257
[12] Manjappa M, Pitchappa P, Singh N, Wang N, Zheludev N I, Lee C and Singh R 2018 *Nat. Commun.* **9** 4056
[13] Geim A K and Novoselov K S 2007 *Nat. Mater.* **6** 183
[14] Bonaccorso F, Sun Z, Hasan T and Ferrari A C 2010 *Nat. Photon.* **4** 611
[15] Bao Q and Loh K P 2012 *ACS Nano* **6** 3677
[16] Lee S H, Choi M, Kim T T, Lee S, Liu M, Yin X, Choi H K, Lee S S, Choi C G, Choi S Y, Zhang X and Min B 2012 *Nat. Mater.* **11** 936
[17] Sensale-Rodriguez B, Yan R, Kelly M M, Fang T, Tahy K, Hwang W S, Jena D, Liu L and Xing H G 2012 *Nat. Commun.* **3** 780
[18] Sensale-Rodriguez B, Yan R, Rafique S, Zhu M, Li W, Liang X, Gundlach D, Protasenko V, Kelly M M, Jena D, Liu L and Xing H G 2012 *Nano Lett.* **12** 4518
[19] Valmorra F, Scalari G, Maissen C, Fu W, Schonenberger C, Choi J W, Park H G, Beck M and Faist J 2013 *Nano Lett.* **13** 3193
[20] Degl'Innocenti R, Jessop D S, Shah Y D, Sibik J, Zeitler J A, Kidambi P R, Hofmann S, Beere H E and Ritchie D A 2014 *ACS Nano* **8** 2548
[21] Gao W, Shu J, Reichel K, Nickel D V, He X, Shi G, Vajtai R, Ajayan P M, Kono J, Mittleman D M and Xu Q 2014 *Nano Lett.* **14** 1242
[22] Mao Q, Wen Q Y, Tian W, Wen T L, Chen Z, Yang Q H and Zhang H W 2014 *Opt. Lett.* **39** 5649
[23] Liang G Z, Hu X N, Yu X C, Shen Y D, Li L H H, Davies A G, Linfield E H, Liang H K, Zhang Y, Yu S F and Wang Q J 2015 *ACS Photon.* **2** 1559
[24] Shi S F, Zeng B, Han H L, Hong X, Tsai H Z, Jung H S, Zettl A, Crommie M F and Wang F 2015 *Nano Lett.* **15** 372
[25] Wu Y, La-o-vorakiat C, Qiu X, Liu J, Deorani P, Banerjee K, Son J, Chen Y, Chia E E and Yang H 2015 *Adv. Mater.* **27** 1874
[26] Jessop D S, Kindness S J, Xiao L, Braeuninger-Weimer P, Lin H, Ren Y, Ren C X, Hofmann S, Zeitler J A, Beere H E, Ritchie D A and Degl'Innocenti R 2016 *Appl. Phys. Lett.* **108** 171101
[27] Kim T T, Kim H, Kenney M, Park H S, Kim H D, Min B and Zhang S 2018 *Adv. Opt. Mater.* **6** 1700507
[28] Jung H, Koo J, Heo E, Cho B, In C, Lee W, Jo H, Cho J H, Choi H, Kang M S and Lee H 2018 *Adv. Mater.* **30** 1802760
[29] Liu P Q, Luxmoore I J, Mikhailov S A, Savostianova N A, Valmorra F, Faist J and Nash G R 2015 *Nat. Commun.* **6** 8969
[30] Miao Z Q, Wu Q, Li X, He Q, Ding K, An Z H, Zhang Y B and Zhou L 2015 *Phys. Rev. X* **5** 041027

[31] Wen Q Y, Tian W, Mao Q, Chen Z, Liu W W, Yang Q H, Sanderson M and Zhang H W 2015 *Sci. Rep.* **4** 7409

[32] Weis P, Garcia-Pomar J L, Hoh M, Reinhard B, Brodyanski A and Rahm M 2012 *ACS Nano* **6** 9118

[33] Tang Y, Zhu Z, Zhang J, Guo C, Liu K, Yuan X and Qin S 2015 *Chin. Phys. Lett.* **32** 025202

[34] Jiang R, Wu Z, Han Z and Jung H 2016 *Chin. Phys. B* **25** 106803

[35] Du L, Li Q, Li S, Hu F, Xiong X, Li Y, Zhang W and Han J 2016 *Chin. Phys. B* **25** 027301

[36] Du X, Skachko I, Barker A and Andrei E Y 2008 *Nat. Nanotechnol.* **3** 491

[37] Novoselov K S, Geim A K, Morozov S V, Jiang D, Zhang Y, Dubonos S V, Grigorieva I V and Firsov A A 2004 *Science* **306** 666

[38] Luo Z T, Pinto N J, Davila Y and Johnson A T C 2012 *Appl. Phys. Lett.* **100** 253108

[39] Kim T T, Oh S S, Kim H D, Park H S, Hess O, Min B and Zhang S 2017 *Sci. Adv.* **3** e1701377

[40] Kindness S J, Almond N W, Wei B B, Wallis R, Michailow W, Kamboj V S, Braeuninger-Weimer P, Hofmann S, Beere H E, Ritchie D A and Degl'Innocenti R 2018 *Adv. Opt. Mater.* **6** 1800570

[41] Kim T T, Kim H D, Zhao R, Oh S S, Ha T, Chung D S, Lee Y H, Min B and Zhang S 2018 *ACS Photon.* **5** 1800

[42] Liu W G, Hu B, Huang Z D, Guan H Y, Li H T, Wang X K, Zhang Y, Yin H X, Xiong X L, Liu J and Wang Y T 2018 *Photon. Res.* **6** 703

[43] Ahmadivand A, Gerislioglu B and Ramezani Z 2019 *Nanoscale* **11** 8091

[44] Jung H, Jo H, Lee W, Kim B, Choi H, Kang M S and Lee H 2019 *Adv. Opt. Mater.* **7** 1801205

[45] Ju L, Geng B, Horng J, Girit C, Martin M, Hao Z, Bechtel H A, Liang X, Zettl A, Shen Y R and Wang F 2011 *Nat. Nanotechnol.* **6** 630

[46] Daniels K M, Jadidi M M, Sushkov A B, Nath A, Boyd A K, Sridhara K, Drew H D, Murphy T E, Myers-Ward R L and Gaskill D K 2017 *2D Mater.* **4** 025034

[47] Castro Neto A H, Guinea F, Peres N M R, Novoselov K S and Geim A K 2009 *Rev. Mod. Phys.* **81** 109

[48] Dawlaty J M, Shivaraman S, Strait J, George P, Chandrashekhar M, Rana F, Spencer M G, Veksler D and Chen Y Q 2008 *Appl. Phys. Lett.* **93** 131905

[49] Chen P Y and Alu A 2011 *ACS Nano* **5** 5855

[50] Nair R R, Blake P, Grigorenko A N, Novoselov K S, Booth T J, Stauber T, Peres N M and Geim A K 2008 *Science* **320** 1308

[51] Liu M, Yin X, Ulin-Avila E, Geng B, Zentgraf T, Ju L, Wang F and Zhang X 2011 *Nature* **474** 64

[52] Polat E O and Kocabas C 2013 *Nano Lett.* **13** 5851

[53] Li Q, Cong L, Singh R, Xu N, Cao W, Zhang X, Tian Z, Du L, Han J and Zhang W 2016 *Nanoscale* **8** 17278

[54] Fedotov V A, Rose M, Prosvirnin S L, Papasimakis N and Zheludev N I 2007 *Phys. Rev. Lett.* **99** 147401

[55] Liu H T, Liu Y Q and Zhu D B 2011 *J. Mater. Chem.* **21** 3335

[56] Kakenov N, Balci O, Takan T, Ozkan V A, Akan H and Kocabas C 2016 *ACS Photon.* **3** 1531

[57] Kakenov N, Ergoktas M S, Balci O and Kocabas C 2018 *2D Mater.* **5** 035018

[58] Chen X, Tian Z, Lu Y, Xu Y, Zhang X, Ouyang C, Gu J, Han J and Zhang W 2019 *Adv. Opt. Mater.* **8** 1900660

[59] Chen X, Tian Z, Wang J, Yuan Y, Zhang X, Ouyang C, Gu J, Han J and Zhang W 2019 *Carbon* **155** 514

[60] Kim J T, Choi H, Choi Y and Cho J H 2018 *ACS Appl. Mater. Interfaces* **10** 1836

[61] Li Q, Tian Z, Zhang X Q, Xu N N, Singh R J, Gu J Q, Lv P, Luo L B, Zhang S, Han J G and Zhang W L 2015 *Carbon* **90** 146

[62] Li Q, Tian Z, Zhang X, Singh R, Du L, Gu J, Han J and Zhang W 2015 *Nat. Commun.* **6** 7082

[63] Qi J, Zhang H, Ji D, Fan X, Cheng L, Liang H, Li H, Zeng C and Zhang Z 2014 *Adv. Mater.* **26** 3735

[64] Gorecki J, Apostolopoulos V, Ou J Y, Mailis S and Papasimakis N 2018 *ACS Nano* **12** 5940

[65] Hwang H Y, Brandt N C, Farhat H, Hsu A L, Kong J and Nelson K A 2013 *J. Phys. Chem. B* **117** 15819

[66] Hafez H A, Lévesque P L, Al-Naib I, Dignam M M, Chai X, Choubak S, Desjardins P, Martel R and Ozaki T 2015 *Appl. Phys. Lett.* **107** 251903

[67] Li S, Nugraha P S, Su X, Chen X, Yang Q, Unferdorben M, Kovacs F, Kunsagi-Mate S, Liu M, Zhang X, Ouyang C, Li Y, Fulop J A, Han J and Zhang W 2019 *Opt. Express* **27** 2317

[68] Kakenov N, Takan T, Ozkan V A, Balci O, Polat E O, Altan H and Kocabas C 2015 *Opt. Lett.* **40** 1984

[69] Watts C M, Shrekenhamer D, Montoya J, Lipworth G, Hunt J, Sleasman T, Krishna S, Smith D R and Padilla W J 2014 *Nat. Photon.* **8** 605